# Isotopic Tracing of Oxygen During Thermal Growth of Thin Films of $SiO_2$ On Si in dry $O_2$

I. Trimaille and J.-J. Ganem

*Groupe de Physique des Solides,*

*URA17-CNRS, Universités Paris 7 et Paris 6*

*75251 Paris CEDEX 05, France*

Received February 22, 1997

The present contribution summarizes the main results of isotopic tracing concerning the atomic transport during growth of very thin (<10 nm) $SiO_2$ films in dry $O_2$. The tracing experiments are combined with nuclear reactions analysis leading to high resolution depth profiling. The growth mechanisms are discussed in terms of the injection of silicon atoms from the substrate, and/or silicon clusters formation, as well as defects migration and interface roughness.

## I. Introduction

The Deal and Grove[1] model is generally accepted for a description of the oxidation of silicon in dry $O_2$ in the case of $SiO_2$ films thicker than 20 nm, although significant deviations occur for the growth kinetics at low pressure or low temperature[2,3]. In the case of thin oxides (below 20 nm) deviations from this model are observed, even at high temperatures and/or pressures, due to an enhancement of the growth rate in the early stages of oxidation[1]. Many models[2,4–8] based on kinetics data were proposed to account for these deviations. Among the numerous models proposed to explain oxide growth in the very thin regime, none has yet been accepted as more valid than the others. In the process simulation software ATHENA[9], the semi-empirical model of Massoud et al[10], that yields reasonable agreement with kinetic data for thicknesses above 5-10 nm is implemented. In this model, a growth rate term, that decays exponentially with thickness and containing three independant parameters, is added to account for the accelerated initial growth. When the thickness of $SiO_2$ films is reduced below 10 nm, modellization of thermal growth requires a larger number of fitting parameters, in particular because the oxidation process becomes strongly dependent on the features of the $SiO_2$/Si interface[2]. Another important aspect which must be investigated is the influence of the roughness of the Si substrate on the initial stages of the oxidation process. Moreover, since the roughness of the $SiO_2$/Si interface was seen to depend on the preoxidation cleaning procedure[2], the role of substrate cleaning on the growth mechanisms of thin $SiO_2$ films should also be investigated. Therefore, for an accurate modellization needed for deep submicron devices, analysis of kinetics data have to be complemented by various types of experiments capable of identifying and quantifying the key parameters controlling growth in the early stages of silicon oxidation.

Isotopic tracing of oxygen is well suited to contribute to the understanding of silicon oxidation in the early stages stages since it brings crucial informations on atomic transport during growth. The present contribution studies the dry oxidation of silicon for films thinner than 10 nm by means of isotopic tracing experiments in combination with nuclear reactions analysis (NRA) leading to high resolution depth profiling.

The atomic transport mechanisms involved in the growth of $SiO_2$ films thicker than 20 nm were previously studied in our laboratory using isotopic tracing experiments. As many aspects of the atomic transport involved in the growth of these thicker films are still relevant when the case of very thin films is considered, an update of the main results of isotopic tracing concerning these thicker films is presented as a basis to discuss the mechanisms of thermal growth in the case of very thin films.

## II. Methods

The principles of isotopic tracing have been exposed in detail in previous publications[11,12]: in the case of dry thermal oxidation, a silicon oxide film is first grown in natural $O_2$ (99.759 % of $^{16}O$, 0.037 % of $^{17}O$, 0.204 % of $^{18}O$), hereafter called $^{16}O_2$, and then in $O_2$ highly enriched (~98 %) in $^{18}O$, called $^{18}O_2$. The various possibles growth mechanisms can be associated with different $^{18}O$ concentration versus depth profiles in the oxide films, that is, plots of the $^{18}O$ local concentration ($[^{18}O][^{18}O+^{16}O]$) in the oxide films (see Fig. 1). Therefore the knowledge of these profiles leads to the investigation of growth mechanisms taking place, which must be also consistent with the kinetic data.

The atomic areal densities of $^{16}O$ and $^{18}O$ in the $SiO_2$ films were determined by non resonant nuclear reaction analysis. General principles of dosing by NRA have been detailed by Amsel et al.[13]. The following reactions were used in the present work at non resonant energies:

$^{18}O(p,\alpha)^{15}N$, induced by a proton beam of 0.73 MeV, with a detection at 150° [13]

$^{16}O(d,p0)^{17}O$, induced by a deuteron beam of 0.81 MeV, with a detection at 90° [14].

The number of detected particles ($\alpha$ or p, respectively) is proportional to the atomic areal densities of $^{16}O$ or $^{18}O$ in the film. The absolute values are determined within 3% by comparison with standards. The detection limit is about $10^{13}$ at.cm$^{-2}$ for $^{18}O$, and $10^{14}$ at.cm$^{-2}$ for $^{16}O$ [15]. The areal densities of oxygen can be converted into equivalent $SiO_2$ thicknesses: by assuming a density of 2.21 g. cm$^{-3}$ for the $SiO_2$ film, $10^{15}$ O at.cm$^{-2}$ correspond to 0.226 nm of $SiO_2$.

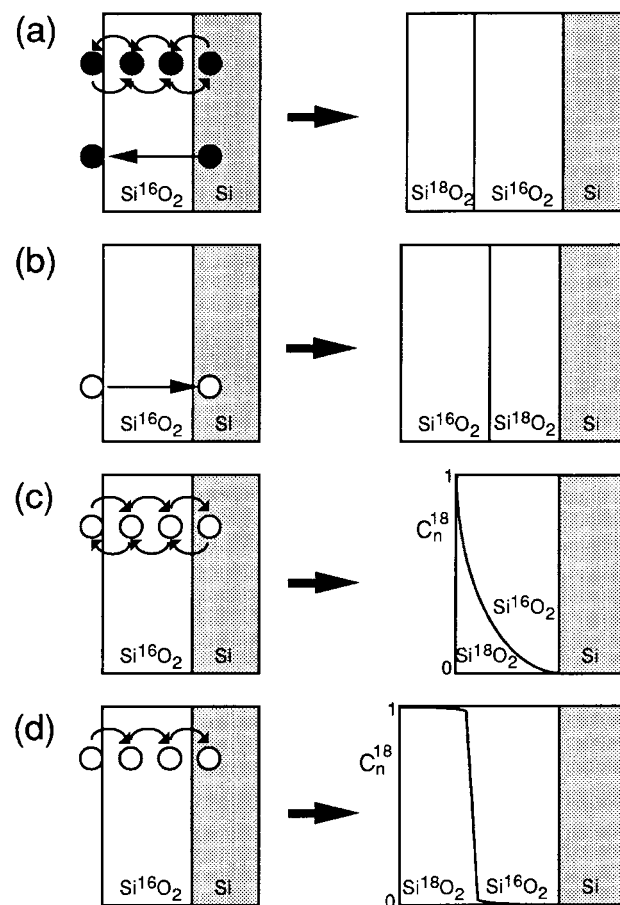


Figure 1. Illustration of how the labelling technique can be used to identify the mobile species and their transport mechanisms. Silicon is first oxidized in natural oxygen and then in oxygen highly enriched in $^{18}O$. Four types of atomic transport are represented as well as the corresponding $^{18}O$ depth profiles: (a) only silicon is mobile; (b) only oxygen is mobile and moves interstitially without reacting with the silica network; (c) only oxygen is mobile and is transported by a step-by-step motion of network oxygen atoms, in a simple diffusion process; (d) only oxygen is mobile and is transported by a step-by-step motion of network oxygen atoms, only in the direction of the growth. Black dots stand for silicon, white dots for oxygen.

We used two methods for the depth profiling. The first one is a step-by-step chemical etching combined with non resonant nuclear reactions analysis, while the second one is high resolution depth profiling using the very narrow (~100 eV) nuclear resonance of the $^{18}O(p,\alpha)^{15}N$ reaction at 151 keV. In the first method, the sample is cut into several pieces which undergo dips

in an etching solution based on hydrofluoric acid (HF) for increasing time intervals, in order to remove increasing thicknesses of the oxide film. The amounts of $^{16}O$ and $^{18}O$ atoms remaining in the samples are measured in each piece using the reactions described above. From these data, the profiles of $^{16}O$ and $^{18}O$ are deduced[16] with a depth resolution of about 2 nm. The nuclear reaction resonance used in the second method was already studied in detail[17] and its application to high resolution depth profiling of $^{18}O$ was demonstrated in ref.18. The number of detected $\alpha$-particles as a function of the energy of the incident proton beam (excitation curve) is recorded for energies above the energy of the resonance. This excitation curve is an image of the $^{18}O$ depth profile, which can be extracted using SPACES, a personal computer implementation of the stochastic theory of energy loss[19,20], and the GENPLOT program[21], used to perform the convolutions of the various components contributing to an excitation curve[22]. The depth resolution in this case is better than 1 nm near the surface in a grazing incidence geometry[18]. The high depth resolution is the consequence of the low width of the resonance ( ~100 eV) associated to the high value of the stopping power in silicon oxide for protons at these low energies (475 keV/(mg.cm$^{-2}$) at 150 keV [18] corresponding to $10^5$ eV/nm). An example of this high near surface sensitivity is shown in Fig. 2, where the excitation curve and two different simulations from a silicon oxide sample with 10.7 × $10^{15}$ $^{18}O$ at.cm$^{-2}$ near the external surface of the film are presented. The sensitivity of the resonance allows one to distinguish clearly an erfc profile from a rectangular profile near the surface (see Fig. 2).

It has to be noticed that oxygen measurements using NRA cannot be performed accurately on boron-doped silicon samples. This is due to the presence of the 300 keV- wide resonance of $^{11}B(p,\alpha)^8Be$ at 662 keV [23].

An alternative mean to achieve high resolution depth profiling is Medium- Energy Ion Scattering[24], which allows profiling of both isotopes of oxygen.

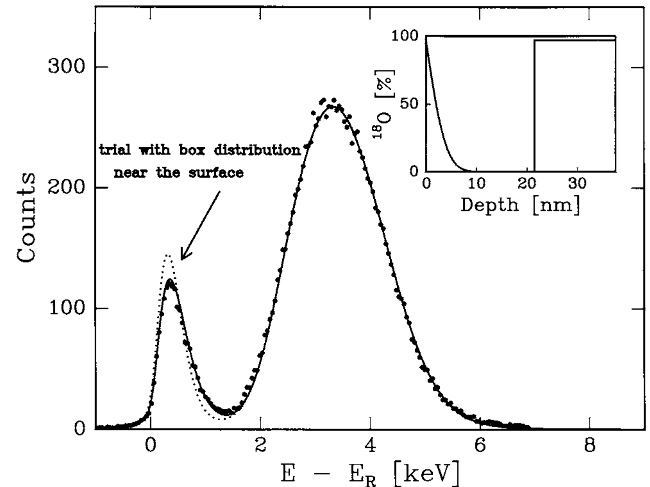


Figure 2. Excitation curve of the $^{18}O(p,\alpha)^{15}N$ nuclear reaction at 151 keV recorded in perpendicular geometry for a $SiO_2$ film grown first in natural oxygen at 1000°C in natural oxygen up to 20.5 nm and reoxidized under 10 kPa of 97% $^{18}O$ enriched oxygen at 930°C for 5 h. The $^{18}O$ depth profile used for the simulation (solid line) of the experimental curve is shown also in the figure: at the external surface the $^{18}O$ depth profile assumed is an erfc with a surface concentration of 97% and $(D^*t)^{1/2}$ equal to 2.2 nm, near the $SiO_2$-Si interface, the $^{18}O$ concentration is constant and equal to 97%. The dot line represents the simulation of the excitation curve when the erfc distribution near the surface is replaced by a rectangular profile of same area and same surface $^{18}O$ concentration.

## III. Experimental procedures

The thin oxides were grown on 2" Si(001) wafers, phosphorus-doped, with nominal resistivity 1-10 Ω.cm, in a ultra-high vacuum technology rapid thermal furnace[14], where a background vacuum in the $10^{-6}$ Pa range is reached in the oxidation zone, before introduction of a controlled static pressure of oxygen. The set-up, schematically represented on Fig. 3, recieves 2" or 3" silicon wafers in a storage chamber. A valve isolates the quartz tube from air during introduction of the wafers in the storage chamber. The two handlers are used to place one wafer on the mobile sample holder in the quartz tube. When the quartz tube is isolated from the storage chamber by closing the valve, the oxidizing gas may then be introduced in the tube. The mobile sample holder allows to put the wafer inside the furnace where it is oxidized. A mass spectrometer permits to analyse the labelled oxidizing gas. The $^{18}O_2$ or $^{16}O_2$ oxidations above 20 nm were performed, for most of them, in a set-up of similar type build around a conventional Joule effect furnace[3].

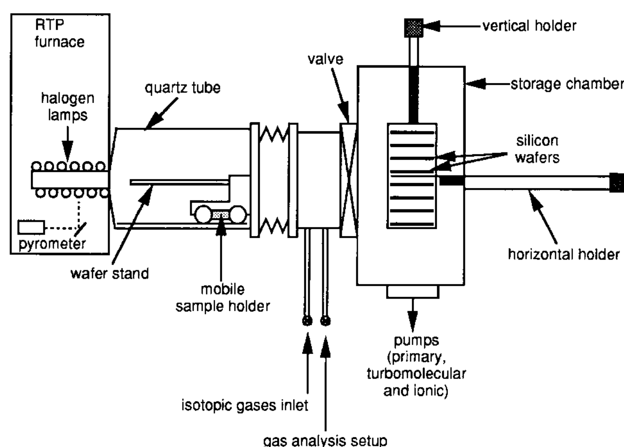


Figure 3. Schematic drawing of ultra high vaccum technology RTP furnace used for sequential $^{16}O/^{18}O$ oxidations.

Prior to oxidation, the silicon substrate is submitted either to a hydrofluoric acid (HF) -based wet cleaning or a rapid thermal cleaning (RTC) performed in situ at 1100°C for 5 s under a residual pressure lower than $10^{-5}$ Pa.

## IV. Growth mechanisms for silicon oxide films thicker than 20 nm

In this section will be reviewed and updated the major results established through isotopic tracing experiments for thick films (20-260 nm) grown in the conventional furnace. The oxidations were performed at temperatures ranging from 880 °C to 1090 °C. Static pressures of $O_2$ were in the range 4 - $10^4$ Pa.

Fig. 4 shows a typical excitation curve of the narrow resonance at 151 keV of the $^{18}O(p,\alpha)^{15}N$ reaction for these films, as well as the $^{18}O$ depth profile used for the simulation of the experimental curve. The heavy isotope is mainly found near the external surface and at the $SiO_2$/Si interface. The $^{18}O$ concentration in the bulk of the $SiO_2$ film is 0.2 % [12,16], which corresponds to the natural abundance of the heavy isotope. Near the external surface, $^{16}O$-$^{18}O$ isotopic exchange is observed. There is no measurable $^{16}O/^{18}O$ mixing at the boundary between the $^{16}O$-rich oxide layer and the $^{18}O$-rich oxide layer closer to the $SiO_2$/Si interface. The $^{18}O$ labeling of the $^{18}O$-rich oxide layer at the $SiO_2$/Si interface is constant and equal to that of the the gas within 0.5 % [16,25].

On the other hand, in the surfacial region, the $^{18}O$ concentration is distributed within the $^{16}O$-rich layer as a complementary error function, with origin at the surface and a $^{18}O$ labelling at the surface equal to that of the gas.

These results evidence two different and non-correlated mechanisms for the fixation of the oxidizing species. In the first one, the heavy isotope goes through the pre-existing oxide matrix without any measurable interaction with it (the $^{18}O$ in the bulk of the $SiO_2$ film has always been found in its natural abundance), reacting with Si atoms from the substrate and beeing fixed near the interface, promoting film growth. This mechanism is in accordance with the Deal and Grove theory which assumes an interstitial diffusion of $O_2$ molecules. The fixation near the oxide surface, consisting in a few $10^{15}$ $^{18}O$ atoms/cm$^2$, occurs due to a mechanism related with a step-by-step motion of network oxygen atoms, by a simple diffusion process, induced by the presence of network defects essentially created near the external surface[16,26].

It was observed an increase in the amounts of $^{18}O$ found near the external surface (FNES), when the initial oxide thickness decreases[16]. This dependence on the thickness was also observed by Han et Helms[27], using Secondary Ion Mass Spectroscopy. The amount $N_s$ of $^{18}O$ FNES is equal to[28]:

$$N_s = \frac{2\sqrt{D^*t}}{\sqrt{\pi}} C_s^{18}, \quad \text{with} \quad D^* = D_d \frac{C_d}{N_N}$$

where $C_s^{18}$ is the $^{18}O$ surface concentration, $t$ is the duration of the $^{18}O_2$ oxidation, $D^*$ is the effective diffusion coefficient of $^{18}O$, $D_d$ and $C_d$ are respectively, the diffusion coefficient and the concentration of the defects, and NN is the oxygene atoms concentration of the silica network. Therefore, an increase of the $^{18}O$ FNES is due to an increase either of the diffusion coefficient of the defects, or of their concentration. In this range of thicknesses, an increase of defect concentration due to a greater supply of electrons from the substrate, is unlikely to explain this thickness dependence. The variation in the amount of $^{18}O$ FNES with the oxide thickness could then be interpreted as: (i) a structural change during the growth, (ii) an enhancement of defect concentration in connection with the growth rate. This last hypothesis has been ruled out by measuring amounts of $^{18}O$ FNES, after the same treatment under

$^{18}O_2$, on two kinds of samples of the same initial thicknesses, but of very different growth rates (the growth on one kind of samples was widely inhibited by a few $10^{15}$ $N^+.cm^{-2}$ implanted at the $SiO_2/Si$ interface after the oxide growth in $^{18}O_2$)[29]. The amounts of $^{18}O$ FNES as well as the $^{18}O$ depth profiles were identical on the two types of samples, whereas the interface growth rate was 25 times slower on the samples with nitrogen. These amounts were measured through step-by-step dissolution combined with non resonant NRA[29], and by resonant NRA[30]. This result also evidences the independence of the two mechanisms responsible for the fixation of $^{18}O$ atoms in the $SiO_2$ film.

To investigate these defects, a study of the amounts of $^{18}O$ FNES as a function of oxidation pressure (4 to $10^4$ Pa) under $^{18}O_2$ was carried out[12]. These amounts support a $P_{O_2}^{1/4}$ law. This favours, among the defects relevant to atomic diffusion[31], the peroxyl bridge (O-O bond, equivalent to an interstitial oxygen atom) as the defect responsible for the step-by step motion of oxygen atoms. To show this, we state that the peroxyl bridge is formed by the reaction:

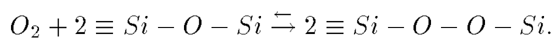

$$O_2 + 2 \equiv Si - O - Si \rightleftharpoons 2 \equiv Si - O - O - Si.$$

Owing to the law of mass action, for a transport by peroxyl bridge, the concentration of defects will be roportionnal to the square root of the $O_2$ pressure, and therefore Ns will be proportionnal to $PO_2^{1/4}$.

The areal density of intrinsic EX centers, determined by electron-spin resonance and interpreted in terms of an oxygen-excess center located within 4 nm of the external surface was also seen to increase as the oxide thickness decreases[32,33]. The peroxyl bridge may be related to the presence of these paramagnetic centers.

Under the supposition of a concentration gradient for the defects, a part of $^{18}O$ FNES participates of the growth. Based on calculations of the total flux of oxygen atoms due to the network defects during the thermal treatment, apart of isotopic exchange, if a concentration gradient of the defects exists a part of $^{18}O$ FNES will take part on the film growth[12]. The growth related to the network defects was quantified in Ref.12. Within the frame of these experiments, it lies between $3 \times 10^{-4}$ and $9 \times 10^{-2}$, evidencing that the film growth occurs essentially due to the other mechanism, the one characterized by Deal and Grove. Summarizing, the growth related to the network defects is expected to increase linearly with the oxidation time and with the square root of $^{18}O_2$ pressure. It increases also when the initial oxide thickness is decreased and when the oxidation temperature is increased. The results of Costello and Tressler[34] evidenced this trend of the temperature dependence. They performed $^{16}O$-$^{18}O$ sequential oxidations at 1300°C and observed a constant profile throughout the oxide film for the $^{18}O$ concentration, the growth probably occurring essentially by defects diffusion.

Under the assumption that these two mechanisms are still those involved for thinner films ($\sim$ 5 nm), extrapolations of our results to this thickness range suggest that oxidations at atmospheric pressure, even at temperatures as high as 1100°C, will produce films where the growth by defects diffusion should not exceed a few percent of the total growth. On the other hand, for oxidations carried out at much lower pressure ($10^2$ Pa or less) and at temperature above 1000°C, the fixation of oxygen due to defects diffusion might be the dominant mechanism. Therefore, we want to point out here that there is a competition in the relative importance of these mechanisms in which the oxidation parameters play a major role.

## V. Isotopic tracing experiments for silicon oxide films thinner than 10 nm

The growth mechanisms of very thin films grown in the ultra-high vacuum conventional Joule effect heated furnace have been also previously studied in our laboratory at lor temperature and/or pressure[3]. In this section, however, only the $^{18}O$ depth profiles in very thin $SiO_2$ films grown in the RTP furnace will be presented. While for thicker oxides the oxygen pressure, substrate orientation and oxidation temperature are the main parameters governing the oxidation process and therefore the oxide quality, for thinner oxides the wafer cleaning process becomes a key step in obtaining high quality oxides[2,35,36].

In order to investigate the effect of the silicon substrate cleaning procedures and of the growth parameters on the oxidation process, we have chosen three different wafer cleaning procedures prior to oxidation:

i) $HF/H_2O$: a dip in HF 48% in water for 30 s followed by a rinse in deionised water for another 30 s ; ii) HF/ethanol: a dip in HF diluted at 4 % in ethanol for 30 s followed by a rinse in ethanol for another 30 s ; and iii) rapid thermal cleaning (RTC) performed in situ at 1100°C for 5 s under a base pressure lower than $10^{-5}$ Pa. The choice of these cleaning procedures aimed the comparison of the atomic transport during oxidation of silicon substrates presenting different surface roughness. It is known that the HF/ethanol cleaning minimizes the roughness of the silicon surface and improves the electrical properties of the oxide grown over it when compared to a similar sample cleaned by $HF/H_2O$ [37]. Furthermore, a previous study of the ageing in air at room temperature of clean Si surfaces (amount of oxygen atoms fixed on the surface exposed to air as a function of time) prepared by various wet cleaning procedures 38 showed that HF/ethanol leads to only 0.25 nm (equivalent thickness) of $SiO_2$ after four hours of exposure to air and to 0.9 nm after 22 days, which was the lowest value found among all tested cleanings procedures. On the other extreme, $HF/H_2O$ presents the highest incorporation of oxygen after four hours (0.45 nm) and this amount was seen to increase steeply up to 1.4 nm after 22 days. These results evidence the very different silicon surface stabilities induced by these two wet cleaning procedures. RTC of the wafers was seen to yield to MOS capacitors exhibiting high leakage current and inhomogeneities in the number of fixed charges in the oxide 39. Fig. 4 and Fig. 5 show the excitations curves of the $^{18}O(p,a)15N$ nuclear reaction near 151 keV, as well as the $^{18}O$ depth profiles obtained from the simulations, for four representative silicon samples. In Fig. 4 the samples were oxidized for 10 s in $^{16}O_2$ then for 20 s in $^{18}O_2$ at 1050 C under 8.4 kPa of oxygen. In (a) the silicon sample was cleaned with HF/ethanol, and in (b) with $HF/H_2O$. In Fig. 5 only the durations of oxidation were modified: 60 s in $^{16}O_2$ followed by 150 s in $^{18}O_2$. To improve the depth resolution for these thin films a tilt angle of 72 between the normal to the sample and the direction of the beam was used. Due to the difficulty in controlling the etching rate for these very thin films, chemical etching in conjunction with NRA of the same samples led to profiles with a worse depth resolution, but still consistent with the ones presented here[40].

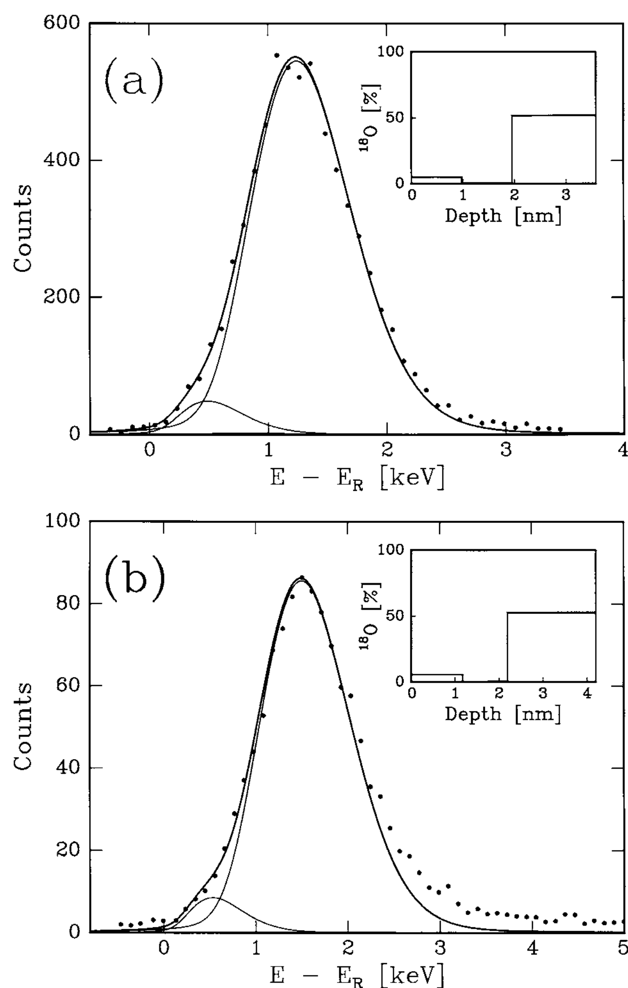


Figure 4. Excitation curve of the $^{18}O(p,\alpha)^{15}N$ nuclear reaction at 151 keV obtained on $SiO_2$ films grown for 10 s under $^{16}O_2$ and then 20 s under $^{18}O_2$. The oxidations of the wafers were performed under 8.4 kPa of oxygen at 1050°C. Prior to oxidation the wafers were submitted to one of the HF-based cleaning procedure described in the text: (a) HF/ethanol; (b) $HF/H_2O$. A tilt angle of 72 between the normal to the sample and the direction of the beam was used to improve depth resolution. The $^{18}O$ depth profiles used for the simulations are shown in the figure.

It is noticeable that the final thicknesses of the $SiO_2$ films depends on the cleaning procedure. RTC leads to thicker oxides than $HF/H_2O$ cleaning 40 and $HF/H_2O$ leads to thicker oxides than HF/ethanol cleaning (see Fig. 4 and Fig. 5).

After the shortest oxidation duration, the two wet cleaning procedures produce similar $^{18}O$ depth profiles: a small amount of $^{18}O$ (about $3\times10^{14}$ $cm^{-2}$) is fixed nearby the surface, while most of the $^{18}O$ is fixed near the interface in an oxide layer composed of about 50 % of $^{18}O$ and 50 % of $^{16}O$. The high energy tail, in the case of of the $HF/H_2O$ cleaned sample, not fitted, may be attributed to the high topographical surface roughness

of the sample.

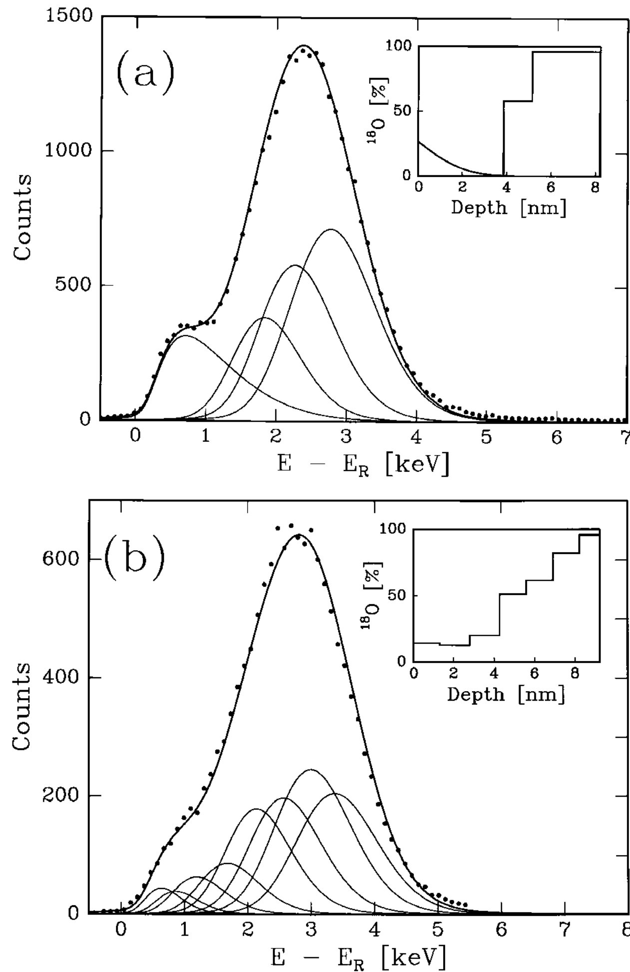


Figure 5. Excitation curve of the $^{18}O(p,\alpha)^{15}N$ nuclear reaction at 151 keV obtained on $SiO_2$ films grown for 60 s under $^{16}O_2$ and then 150 s under $^{18}O_2$. The oxidations of the wafers were performed under 8.4 kPa of oxygen at 1050°C. Prior to oxidation the wafers were submitted to one of the HF-based cleaning procedure described in the text: (a) HF/ethanol; (b) HF/$H_2O$. A tilt angle of 72° between the normal to the sample and the direction of the beam was used to improve depth resolution. The $^{18}O$ depth profiles used for the simulations are shown in the figure.

After the longest oxidation duration, in both cases a pure $Si^{18}O_2$ (a $SiO_2$ layer with an isotopic labelling equal to that of the $^{18}O$-enriched gas) is formed near and at the Si-$SiO_2$ interface. Differently from the case of thicker films, presented in the previous section, there is an $^{16}O$-$^{18}O$ mixing in the bulk of the oxide. This mixing was also observed at lower oxygen pressures by Gusev et al. using Medium-Energy Ion Scattering[24]. This mixing is stronger when the silicon surface was cleaned in HF/$H_2O$ compared to HF/ethanol cleaning procedure. RTC is seen to lead to much stronger mixing than HF/$H_2O$ [40]. In the case of the HF/ethanol cleaned sample we estimate the amount of $^{18}O$ fixed near the external surface to $3 \times 10^{15}$ at.cm$^{-2}$.

## VI. Growth mechanisms for silicon oxide films thinner than 10 nm

In the case of silicon oxide films thicker than 20 nm there are apparently two independent mechanisms responsible for the O fixation and film growth: interstitial movement of $O_2$ molecules through the oxide network to react with Si atoms at the interface, and step-by-step motion of O atoms by simple diffusion induced by the presence of network defects near the external surface. For thinner films, the situation seems to be more complex. The $^{18}O$ found near the surface of very thin films of silicon oxide after sequential $^{16}O_2$-$^{18}O_2$ oxidations may be attributed to a mechanism of creation and diffusion of atomic oxygen network defects similar to the one acting in thicker films. However, differently from the case of thick films, the distribution of $^{18}O$ near the surface did not reach a maximum concentration equal to that of the gas, even for oxidation times in $^{18}O_2$ as long as 150 s.

The absence of a pure $Si^{18}O_2$ layer near the interface for films thinner than 5 nm (see Fig. 4) can be explained either by interface roughness or by the injection of silicon atoms from the silicon substrate, as suggested by several authors[41−43]. This last suggestion has some aspects in common with the reactive layer model proposed by Stoneham et al.[44]. In the case of ultra thin films, injected silicon atoms could be still in excess to the $O_2$ molecules. These injected atoms would coalesce to form Si fragments in the oxide during the $^{16}O_2$ oxidation. Finally, these Si clusters would then be oxidized during the $^{18}O_2$ treatment leading to an $^{16}O$-$^{18}O$ mixing. There are experimental evidences by STM (Scanning Transmission Microscopy)[45] and RHEED (Reflection High Energy Electron Diffraction)[3] for silicon clusters formation in ultra thin films of silicon oxide (<1.5 nm). Furthermore, silicon clusters provide additional reaction sites for the $O_2$ molecules and can explain the higher oxidation rates observed in this thickness range. The effect of silicon clusters on the

oxidation rate was modelled assuming spherical silicon clusters[46], leading to an order 3 polynomial oxidation time dependence for the oxide thickness. This model was applied to fit kinetic data for oxides grown in the rapid thermal oxidation furnace at temperatures ranging from 1000°C to 1200°C and under oxygen pressures ranging from 4 to 14 kPa on silicon wafers cleaned by RTC. The parameters extracted from this fitting showed that the areal density of silicon atoms forming the initial clusters and the oxide thickness at which they disappear increase with temperature and oxygen pressure. Based on this model, after 10 s of oxidation at 1050°C, corresponding to oxides thinner than 10 nm, Si fragments should be present in the bulk of the oxide.

A pure $Si^{18}O_2$ layer nearby the interface, resembling the Deal and Grove mechanism, was seen to be formed for the thicker films. However, even for these films, the Deal and Grove mechanism alone cannot account for the $^{18}O$ fixation near the Si- $SiO_2$ interface, since a higher mixing between the $^{16}O$-rich and the $^{18}O$-rich $SiO_2$ layers associated to a higher thickness of the films occur. See Ref.40 for a comparison between $HF/H_2O$ cleaning and RTC: for the same oxidation parameters, RTC was seen to lead to a thicker oxide and to a higher $^{16}O$-$^{18}O$ mixing than $HF/H_2O$ cleaning. The effect of the cleaning procedure on the $^{16}O$-$^{18}O$ mixing can be explained either by a greater interface roughness or by an increase of the oxygen defects density in the bulk of the oxide, but not by the presence of Si clusters. Mobile defects would induce an $^{16}O$-$^{18}O$ mixing between the pure $Si^{18}O_2$ layer near the interface and the bulk of the $Si^{16}O_2$ [16], and a concentration of defects much higher for thinner films would reveal a mixing not observed for thicker films (compare the gradual $^{16}O$-$^{18}O$ boundaries in Fig. 5 with the abrupt one of Fig. 2). The presence of Si fragments cannot account for this mixing since after 60 s of thermal treatment in $^{16}O_2$ their presence was ruled out both by channeling experiments[47], where stoichiometric $SiO_2$ films were observed for such thicknesses, and by the model proposed in Ref. 46, which predicts that Si fragments would be already totally consumed after this oxidation step.

## VII. Conclusion

The isotopic studies presented in this paper allowed us to suggest possible mechanisms involved in the growth of very thin $SiO_2$ films: silicon injection, silicon clusters formation and defects migration. In an attempt to further clarify the intricate phenomena occuring during the first stages of dry oxidation of silicon, in particular silicon injection, isotopic studies using $^{29}Si$ and $^{30}Si$ associated with very narrow nuclear reactions resonances, allowing high depth profiling resolution, should be performed.

For deep submicron technologies, thermal oxynitrides are currently investigated to replace $SiO_2$ grown in oxygen, as gate dielectrics. The narrow resonance ($\sim$ 30 eV) of $^{15}N(p,\alpha)^{12}C$ at 429 keV allows the use of isotopic tracing experiments associated with high resolution depth profiling to investigate on the atomic transport in these oxynitrides.

## Acknowledgements

This work was supported by the Centre National de la Recherche Scientifique, GDR 86.

## References

1. B.E. Deal and A.S. Grove, J. Appl. Phys. **36**, 3770 (1965).
2. C.J. Sofield and A.M. Stoneham, Semicond. Sci. Technol. **10**, 215 (1995).
3. F. Rochet, S. Rigo, M. Froment, C. d'Anterroches, C. Maillot, H. Roulet and G. Dufour, Advances in Physics **35**, 236 (1986).
4. K. Kim, Y.H. Lee, M.H. An, M.S. Suh, C. J. Youn, K. B. Lee and H.J. Lee, Semicond. Sci. Technol. **11**, 215 (1996).
5. S. Dimitrijev, H. B. Harrison, J. Appl. Phys. **80**, 2467 (1996).
6. N.F. Mott, S. Rigo, F. Rochet and A. Stoneham, Phil. Mag. B **60**, 189 (1989).
7. B.E. Deal, in *The Physics and Chemistry of $SiO_2$ and the Si-$SiO_2$ Interface,* edited by C.R. Helms and B.E. Deal (Plenum, New York, 1988), p. 5.
8. J.D. Plummer, in *The Physics and Chemistry of $SiO_2$ and the Si-$SiO_2$ Interface -3*, edited by H.Z. Massoud, E.H. Pointdexter and C.R. Helms (The Electrochemical Society, Pennington, 1996), p. 129.

9. *ATHENA, 2D Process Simulation Software*, Edition 4, Silvaco International, 1996, p.3-34.
10. H.Z. Massoud, J. D. Plummer and E.A. Irene, J. Electrochem. Soc. **132**, 2685 (1985).
11. S. Rigo, in *The Physics and Chemistry of $SiO_2$ and the Si-$SiO_2$ Interface*, edited by C.R. Helms and B.E. Deal (Plenum, New York, 1988), p. 75.
12. I. Trimaille and S. Rigo, Appl. Surf. Sci. **39**, 65 (1989).
13. G. Amsel, J.-P. Nadai, E. d'Artemare, D. David, E. Girard and J. Moulin, Nucl. Instrum. Meth. **92**, 481 (1971).
14. J.-J. Ganem, thèse de doctorat de l'Université Paris 7 (1992).
15. S. Rigo, Nucl. Instrum. Meth. B **64**, 1 (1992).
16. F. Rochet, B. Agius and S. Rigo, J. Electrochem. Soc. **131**, 914 (1984).
17. G. Battistig, G. Amsel, E. d'Artemare and I. Vickridge, Nucl. Instrum. Meth. B **61**, 369 (1991).
18. G. Battistig, G. Amsel, E. d'Artemare and I. Vickridge, Nucl. Instrum. Meth. B **66**, 1 (1992).
19. I. Vickridge and G. Amsel, Nucl. Instrum. Meth. B **45**, 6 (1990).
20. G. Amsel and I. Vickridge, Nucl. Instrum. Meth. B **45**, 12 (1990).
21. *Manual of GENPLOT*, Computer Graphics Service Ltd., Ithaca, NY (1991).
22. I.J.R. Baumvol, F.C. Stedile, J.-J. Ganem, S. Rigo and I. Trimaille, J. Electrochem. Soc. **142**, 1205 (1995).
23. E. Ligeon and A. Bontemps, J. Radioanaly. Chem.**12**, 335 (1972).
24. E.P. Gusev, H.C. Lu, T. Gustafsson and E. Garfunkel, Phys. Rev. B **52**, 1759 (1995).
25. E. Rosencher, A. Straboni, S. Rigo and G. Amsel, Appl. Phys. Lett. **34**, 254 (1979).
26. F. Rochet, thèse de troisième cycle de l'Université Paris 6 (1981).
27. C.J. Han and C.R. Helms, J. Electrochem. Soc. **135**, 1824 (1988).
28. S. Rigo, F. Rochet, B. Agius and A. Straboni, J. Electrochem. Soc. **129**, 867 (1982).
29. I. Trimaille, S. I. Raider, J.-J. Ganem, S. Rigo and N.A. Penebre, in *The Physics and Chemistry of $SiO_2$ and the Si-$SiO_2$ Interface-2,* edited by C.R. Helms and B.E. Deal (Plenum, New York, 1993), p. 7.
30. I. Trimaille, F. C. Stedile, J.-J. Ganem, I.J.R. Baumvol and S. Rigo, in *The Physics and Chemistry of $SiO_2$ and the Si-$SiO_2$ Interface 3,* edited by H.Z. Massoud, E.H. Pointdexter and C.R. Helms (The Electrochemical Society, Pennington, 1996), p. 59
31. J. Robertson, Philosophical Magazine B **55**, 673 (1987).
32. A. Stesmans and F. Scheerlink, J. Appl. Phys. **75**, 1047 (1994).
33. A. Stesmans and F. Scheerlink, Phys. Rev. B**50**, 5204 (1994).
34. J. A. Costello and R.E. Tressler, J. Electrochem. Soc. **131**, 1944 (1984).
35. M. Morita and T. Ohmi, in *The Physics and Chemistry of $SiO_2$ and the Si-$SiO_2$ Interface-2,* edited by C.R. Helms and B.E. Deal (Plenum, New York, 1993), p. 199.
36. M. Chouko and V. Kaushik, in *The Physics and Chemistry of $SiO_2$ and the Si-$SiO_2$ Interface-2,* edited by C.R. Helms and B.E. Deal (Plenum, New York, 1993), p. 267.
37. B. Garrido, F. Gessinn, J.-L. Prom, J. R. Morante, J. Samitier and G. Sarrabayrouse, in *The Physics and Chemistry of $SiO_2$ and the Si-$SiO_2$ Interface-2,* edited by C.R. Helms and B.E. Deal (Plenum, New York, 1993), p. 215.
38. J.-J. Ganem, S. Rigo, I. Trimaille and G. N. Lu, Nucl. Instrum. Meth. B**64**, 784 (1992).
39. E. Slottje and V. Voirot, DEA report, Université Paris 7 (1992).
40. F. C. Stedile, I.J.R. Baumvol, J.-J. Ganem, S. Rigo, I. Trimaille, G. Battistig, W.H. Schulte and H.W. Becker, Nucl. Instrum. Meth. B**85**, 248 (1994).
41. W.A. Tiller, J. Electrochem. Soc. **127**, 619 (1980).
42. S.T. Dunham and J.-D. Plummer, J. Appl. Phys. **59**, 2541 (1986).
43. K. Taniguchi, Y. Shibata and C. Hamaguchi, J. Appl. Phys. **65**, 2723 (1989).
44. A.M. Stoneham, C.R.M. Grovenor and A. Cerezo, Phil. Mag. B**55**, 201 (1987).
45. J.M. Gibson and Lanzerotti, Nature **340**, 128 (1989).
46. J.-J. Ganem, S. Rigo and I. Trimaille, Microelectronic Engineering **22**, 35 (1993)
47. F. C. Stedile, I.J.R. Baumvol, I.F. Oppenheim, I. Trimaille, J.-J. Ganem and S. Rigo, Nucl. Instrum. Meth. B **118**, 493 (1996).